# Notable photocatalytic activity of TiO$_2$-polyethylene nanocomposites for visible light degradation of organic pollutants

*M. Romero-Sáez*[1*]*, L. Y. Jaramillo*[1,2]*, R. Saravanan*[3]*, N. Benito*[4]*, E. Pabón*[2]*, E. Mosquera*[5]*, F. Gracia*[3]

[1]Grupo Calidad, Metrología y Producción, Instituto Tecnológico Metropolitano, Campus Robledo, Calle 73 No. 76A-354, Medellín, Colombia

[2]Grupo Ciencia de Materiales Avanzados, Facultad de Ciencias, Universidad Nacional de Colombia, Sede Medellín, Calle 59A No 63-20, Medellín, Colombia

[3]Laboratorio de Catálisis, Depto. de Ingeniería Química y Biotecnología, FCFM, Universidad de Chile, Beauchef 851, Santiago, Chile

[4]Laboratorio de Superficies, Depto. de Física, FCFM, Universidad de Chile, Av. Blanco Encalada, 2008 Santiago, Chile

[5]Departamento de Física, Universidad del Valle, A.A. 25360, Cali, Colombia

**Abstract.** This paper reports on the photocatalytic activity showed by nanocomposites of TiO$_2$ with low density polyethylene (LDPE) and high density polyethylene (HDPE) (10, 20 wt%) for the degradation of methyl orange in aqueous medium under visible light irradiation. TiO$_2$ was synthetized by sol-gel process, and the polymers were incorporated by impregnation. Both the pure TiO$_2$ and the nanocomposites were characterized using different physico-chemical techniques including specific surface area analysis, X-ray diffraction analysis, transmission electron microscopy, ultraviolet-visible and photoluminescence spectroscopy, and X-ray photoelectron spectroscopy. All the prepared nanocomposites showed an absorption edge in the visible region. TiO$_2$(90)/LDPE photocatalyst showed the best degradation efficiency after 180 minutes of reaction, without notorious decrease of degradation efficiency after three consecutive uses. Photoluminescence and X-ray photoelectron spectroscopy analyses suggested the presence of vacancies in the TiO$_2$ structure promoted by a Ti–O–C interaction being responsible for the photocatalytic activity enhancement under visible light irradiation.

*Keywords: polymer composites, TiO$_2$/LDPE, TiO$_2$/HDPE, photocatalytic activity, visible light*

## 1. Introduction

Environmental pollution is one the key challenges for our modern industrial society. The increasing of toxic compound levels, both in air and water, requires effective methods and techniques for their degradation and/or conversion into harmless species. Advanced oxidation processes (AOPs) are one of the most attractive technologies for wastewater treatment. Among various AOPs, heterogeneous photocatalysis is a promising method for the degradation of various organic pollutants in wastewater [1–3].

Titanium dioxide has been the most studied photocatalyst for the oxidation of organic contaminants in wastewaters. This semiconductor is a very well-known and well researched material due to the stability of its chemical structure, biocompatibility, low cost and optical and electrical properties [4, 5]. Among the most important applications of TiO$_2$ as photocatalyst

---

*Corresponding author, e-mail: manuelromero@itm.edu.co

are self-cleaning and self-sterilizing surfaces [6], water [7] and air purification [8]. However, although $TiO_2$ is a reference material in UV photocatalysis, it is inactive in the visible region due to its wide band gap (~3.2 eV), rendering it less efficient for its use in solar photocatalysis [4, 5]. Several methods have been applied to improve the $TiO_2$ photocatalytic efficiency, like surface modification via organic materials [1, 2], semiconductor coupling [9], and band gap modification by creating oxygen vacancies or oxygen deficiency through metal or nonmetal doping [10, 11]. Some studies report that when an oxygen vacancy was introduced in $TiO_2$, mid-gap electronic states derived from hybridization of the O 2p orbital with the Ti 3d orbital were created, and the optical transition between mid-gap states and the conduction band tail would produce charge transfer from the O 2p orbital to the Ti 3d orbital, resulting in a reduced band gap of $TiO_2$ with oxygen vacancy [12, 13].

Polymer-semiconductor composites have received growing attention for their applications in photocatalysts, sensor materials and photoelectric devices [14, 15]. The interpenetration of inorganic and organic phases at nanoscale level is suggested to improve the individual properties in a global synergetic effect [16]. In this work, low density (LDPE) and high density polyethylene (HDPE) were selected as doping phases since they are non-toxic and low cost polymers, with good chemical and thermal stability. In addition, the intrinsic hydrophobicity of these polymers made it possible to obtain floating photocatalysts. Some of the most important advantages of this kind of photocatalysts are that it can effectively improve the usage of visible light, especially in systems using solar irradiation and also it maximizes the oxygenation of the system due to the proximity with the water surface. Other features of floating photocatalysts are that they present higher efficiency in non-stirred reactions, they can be applied directly in the contaminated wastewater located in remote areas without any special installation and they could be recovered after the photocatalytic reaction by phase separation, solving the problem of a hard recycling [17, 18].

This work studies the photocatalytic activity of $TiO_2$ based nanocomposites under visible light. $TiO_2$ and $TiO_2$/LDPE and $TiO_2$/HDPE nanocomposites were synthesized by sol-gel method followed by impregnation, characterized by several techniques and finally, its photocatalytic activity under visible light

irradiation was investigated through degradation of methyl orange dye.

## 2. Methods
### 2.1. Materials
For the synthesis of pure $TiO_2$, titanium (IV) isopropoxide (TTIP), ethanol and citric acid were obtained from Sigma-Aldrich, Schnelldorf (Germany), and were used without further purification. All the aqueous solution was prepared using double distilled water.

LDPE (HP2027LN) was supplied by Sabic, Houston (USA), with a melt flow index (MFI) = 1.9 g·min⁻¹ and density of 0.926 g·cm⁻³. Meanwhile, HDPE was supplied by Ipiranga Petroquimica, Porto Alegre (Brazil), with a MFI = 0.8 g·min⁻¹ and density of 0.958 g·cm⁻³.

For the photocatalytic reaction methyl orange (MO) dye was purchased from Sigma-Aldrich, Schnelldorf (Germany).

### 2.2. Preparation of $TiO_2$ based composites
*Preparation of $TiO_2$*
Nanosized $TiO_2$ was prepared by sol-gel method. 10 mL of TTIP solution was dissolved in 500 mL of ethanol in a 1000 mL beaker. The mixed solution was refluxed overnight. 0.5 mole of aqueous citrate solution was added drop-wise into the refluxed solution. Then, the resulting solution was stirred mechanically during about 24 hours. Thus a gel was obtained. This gel was dried at room temperature for 7 days, removed from the beaker and transferred to the mortar for grinding. The finely ground sample was later transferred into an alumina boat and calcined at 400 °C for 90 minutes in a muffle furnace.

*Preparation of $TiO_2$/LDPE and $TiO_2$/HDPE nanocomposites*
For the preparation of $TiO_2$/PE nanocomposites, the amount of the PE and the $TiO_2$ were weighted previously so as to obtain final catalysts with 10 and 20 wt% PE. The polymer was dissolved in xylene at 90 °C. Then, $TiO_2$ was added and the solvent was slowly evaporated under agitation at 90 °C during approximately 2 hours. The obtained material was dried under vacuum at 90 °C for another 12 additional hours. After this process, powder photocatalysts with different $TiO_2$ (80 and 90 wt%) and LDPE or HDPE (20 and 10 wt%) proportions were obtained. The resulted composites were named $TiO_2(X)$/LDPE

and TiO$_2$(X)/HDPE to indicate the amount of TiO$_2$ and the polymer used in each case.

## 2.3. Characterization details

Surface area of different samples were determined by N$_2$ adsorption-desorption isotherms at –196 °C in a Micromeritics ASAP 2010 equipment. X-ray diffraction (XRD) analyses were carried out at room temperature in a Bruker D8 Advance diffractometer using Cu Kα irradiation at λ = 1.54 Å; the scanning 2θ range was from 10 to 80°, with an increment of 0.02° and time per step of 0.5 s. A Tecnai F20 FEG-S/TEM microscope operated at 200 kV, equipped with an energy dispersive X-ray (EDX) detector was used for transmission electron microscopy (TEM) analyses. The powder samples were dispersed in isopropanol by ultrasonic stirring for 15 min, and the dispersion was dropped in carbon-copper grids. In order to remove organic contamination, the grids were exposed to an argon plasma cleaning before microscopy measurements. Absorbance measurements and concentration of MO solutions were analyzed using a Perkin Elmer UV-Visible spectrophotometer Lambda 11. X-ray photoelectron spectroscopy (XPS) spectra were measured using a hemispherical analyser (Physical Electronics 1257 system). A twin anode (Mg and Al) X-ray source was operated at a constant power of 200 W using Al Kα radiation (1486.6 eV) for the XPS measurements. The sample was placed in a sample stage in which the emission angle can be varied. In this case, the emission angle was 45°. All XPS spectra were calibrated using C 1s band at 285 eV. Photoluminescence (PL) measurements were performed at room temperature in a Perkin-Elmer spectrofluorometer LS-55, equipped with a Xenon lamp.

## 2.4. Photocatalytic reactions

The procedure for photocatalytic activity evaluation has been described elsewhere [19]. The synthesized samples were used as a catalyst for the degradation of MO solution under visible light illumination using a projector lamp (halogen lamp 250 W, Philips, 532 nm) in a homemade photoreactor. The power density of light irradiation at the surface sample was 180±20 mW/cm$^2$. Reaction mixtures were prepared by adding 50 mg of photocatalyst into 500 mL of MO solution, with an initial concentration of $5\cdot10^{-5}$ mol·L$^{-1}$. The photoreactor was irradiated with constant stirring, and samples from the suspension were collected

at regular time intervals, centrifuged and filtered. The pH value was ~8 to 10. The MO concentration was estimated through a calibration curve of the absorbance at 464 nm using UV-visible spectrophotometer. The degradation efficiencies of MO was calculated using the following Equation (1):

$$\eta = \left[1 - \frac{C}{C_0}\right] \cdot 100 \tag{1}$$

where $C_0$ and $C$ are the concentrations of the solution before illumination ($t = 0$) and after illumination of light for '$t$' minutes, respectively.

## 3. Results and discussion
### 3.1. Characterization of photocatalysts

XRD patterns of the synthesized TiO$_2$ and both TiO$_2$/PE nanocomposites are presented in Figure 1. Structure analysis of the pure TiO$_2$ (Figure 1 curve a) exhibited characteristic anatase phase pattern (JCPDS 89–4921), with diffraction peaks at 2 theta values of 25.4° (101), 37.8° (004), 48.2° (200), 53.9° (105), 55.2° (211), 62.8° (204), 69.0° (116), 70.5° (200) and 75.2° (215) [20]. Diffractograms of TiO$_2$/LDPE nanocomposites (Figure 1 curve d and e) showed very similar pattern to anatase, without additional peaks. The typical diffraction peaks for LDPE appear at 2 theta values of 21.1, 23.8 and 36° [21, 22]. This indicated that no change in crystalline structure was produced during the preparation of these photocatalysts. On the other hand, even though the diffractograms corresponding to TiO$_2$/HDPE nanocomposites (Figure 1 curve b and c) showed similar pattern to pure TiO$_2$, additional peaks at 21.6 and 24° were observed. These reflection peaks corresponded
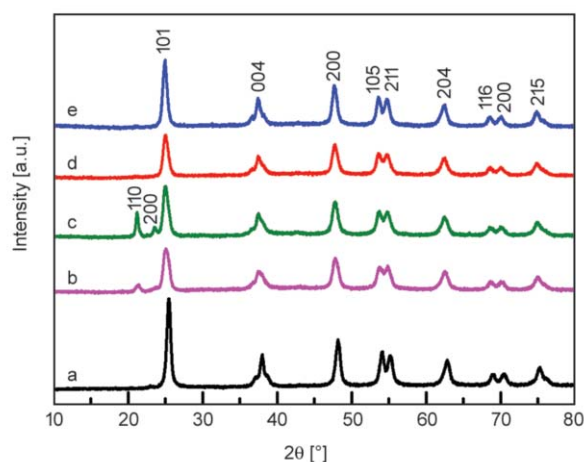


**Figure 1.** XRD pattern of pure TiO$_2$ (a), TiO$_2$(90)/HDPE (b), TiO$_2$(80)/HDPE (c), TiO$_2$(90)/LDPE (d) and TiO$_2$(80)/LDPE (e)

**Table 1.** Values of BET surface area, FWHM, crystallite size (*D*), bandgap, wavelength and degradation efficiency for all synthesized samples

| Sample | BET surface [m²·g⁻¹] | FWHM | Crystallite size[a] *D* [nm] | Band gap values [eV] | Wavelength [nm] | Degradation efficiency after 180 min [%] |
|---|---|---|---|---|---|---|
| TiO₂ | 71 | 0.658 | 22 | 3.31 | 375 | 5 |
| TiO₂(90)/HDPE | 33 | 0.838 | 17 | 3.12 | 397 | 58 |
| TiO₂(80)/HDPE | 21 | 0.899 | 16 | 3.02 | 410 | 45 |
| TiO₂(90)/LDPE | 39 | 0.713 | 20 | 2.98 | 416 | 92 |
| TiO₂(80)/LDPE | 25 | 0.819 | 18 | 2.85 | 435 | 81 |

[a]Calculated by the Debey-Scherrer's formula

to a typical orthorhombic unit cell structure of (110) and (200) reflection planes respectively, corresponding to HDPE [23, 24]. Additionally, as can be observed comparing curves 1b with 1c, the intensity of the HDPE peaks increases with the polymer content. The TiO₂ average crystallite size in pure TiO₂ and within the nanocomposites was calculated using the Debey–Scherrer's formula [25], from line broadening (FWHM) of the (101) diffraction peak. The FWHM values and the crystallite size are listed in Table 1. The TiO₂ crystallite sizes obtained were very similar, with slightly smaller values for the nanocomposites than for pure TiO₂ according to the XRD patterns.

BET surface analyses (Table 1) showed a decrease on surface area when the TiO₂ was combined with both LDPE and HDPE. These results suggested the partial coating of TiO₂ particles with polyethylene, depending on both the type of polyethylene and its concentration in the catalyst. Thus, samples with 20 wt% polyethylene showed lower surface area than those containing 10 wt%. Comparing the type of polymer, TiO₂/HDPE nanocomposites showed slightly lower areas than those obtained with TiO₂/LDPE.
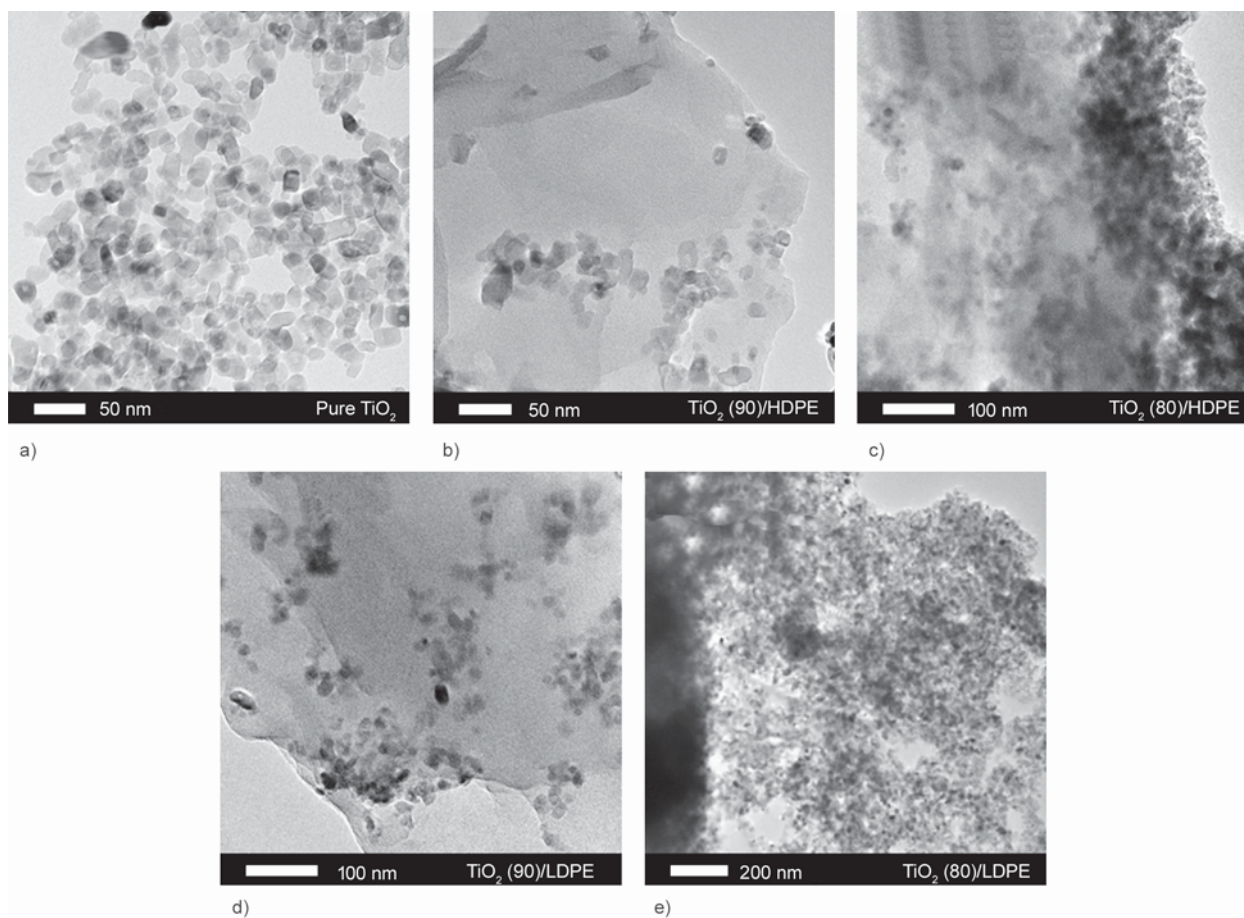


**Figure 2.** TEM analyses of the pure TiO₂ and TiO₂/LDPE and TiO₂/HDPE nanocomposites with 10 and 20 wt% of polymer

TEM images of $TiO_2$ and LDPE and HDPE nanocomposites are shown in Figure 2. The EDX analyses of the nanocomposites (not shown) confirm the presence of the $TiO_2$ nanoparticles into the polymers. The analysis of pure $TiO_2$ showed nanoparticles of about 20 nm, which was consistent with that calculated by Debey-Scherrer's formula (Table 1). The images of the nanocomposites showed two different results, depending on the amount of polymer present in the photocatalyst. Both samples with 10% polyethylene showed good dispersion of $TiO_2$ nanoparticles within the polymer, facilitating a good contact between the $TiO_2$ and the polymer. On the other hand, TEM micrographs of samples with 20% polyethylene were very different from those obtained with 10% polymer, since in these cases both samples showed important $TiO_2$ agglomerates. These results are later correlated with the photocatalytic activity of the samples regarding the effect of polymer concentration on $TiO_2$ nanoparticles dispersion and, consequently, on their MO degradation efficiency.

The optical band gaps of the prepared materials were determined by UV-Vis absorption spectroscopy (Figure 3). $TiO_2$ absorption edge is located around 355 nm, characteristic of an UV active material. The corresponding band gap energies were estimated through Tauc's plot [26], and those results with the corresponding wavelength values are shown in Table 1. It is clear that the band gap value for all nanocomposites is smaller compared to that of pure $TiO_2$. This variation of band gap indicates that the prepared polymer nanocomposites have absorption bands in the visible region, suggesting a synergistic effect between $TiO_2$ and polyethylene due to intermolecular interaction.
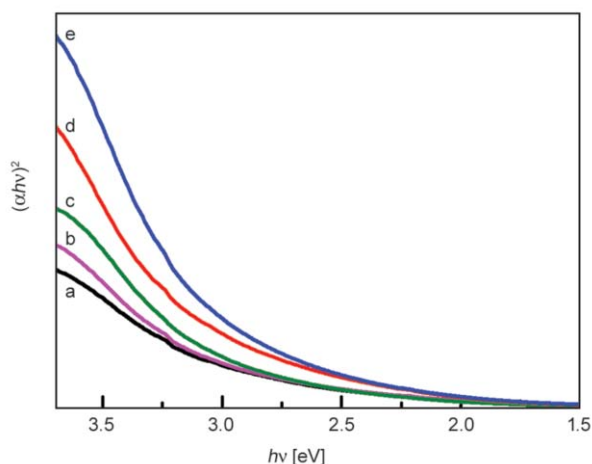


**Figure 3.** UV-Visible absorption spectrum of the pure $TiO_2$ (a), $TiO_2$(90)/HDPE (b), $TiO_2$(80)/HDPE (c), $TiO_2$(90)/LDPE (d) and $TiO_2$(80)/LDPE (e)
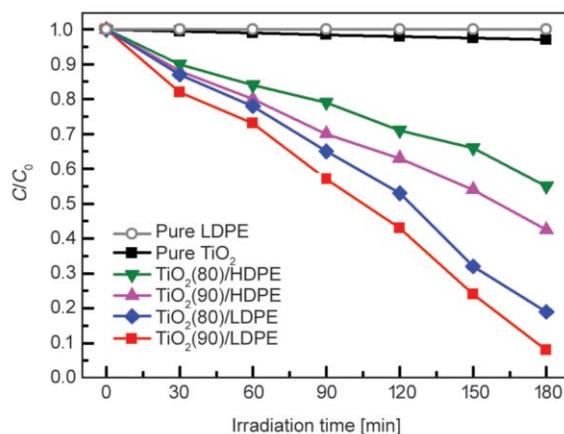


**Figure 4.** Time course methyl orange degradation curve for pure $TiO_2$ and $TiO_2$/LDPE and $TiO_2$/HDPE nanocomposites

## 3.2. Evaluation of photocatalytic activity

The MO degradation curves as a function of irradiation time for all the prepared samples are shown in Figure 4. As expected, it was clearly observed the low degradation activity of pure $TiO_2$ under visible light. Additionally, pure LDPE was also evaluated to confirm its zero activity for MO photo-degradation. Therefore, the photocatalytic activity measured for the prepared nanocomposites was undoubtedly due to the interaction between $TiO_2$ and polyethylene. In fact, the results showed how the MO concentration decreased with irradiation time for all $TiO_2$-PE nanocomposites, corroborating their activity under visible light irradiation.

Table 1 shows the degradation efficiency values for all the prepared samples after 180 minutes. It was observed that $TiO_2$/LDPE nanocomposites showed greater activity than $TiO_2$/HDPE ones. In both cases, the catalysts with 10% polymer showed greater activity, suggesting that the higher dispersion of $TiO_2$ nanoparticles, observed by TEM, favored the activity. Among the different composites studied, $TiO_2$(90)/LDPE showed the highest degradation activity. Nonetheless, besides having the highest surface area of all four composites and a good $TiO_2$ nanoparticles dispersion, the characterization results presented above do not render a clear explanation of the synergy between polymer and $TiO_2$. Therefore, for a better understanding of the interaction between $TiO_2$ and polyethylene in these nanocomposites, XPS measurements of pure $TiO_2$, $TiO_2$(90)/LDPE and $TiO_2$(90)/HDPE samples were carried out. Figure 5a shows Ti 2p band after Shirley background subtraction of fresh $TiO_2$ and nanocomposites.

In the case of pure $TiO_2$, the Ti $2p_{3/2}$ band is centered at 459.0 eV, and can be attributed to $Ti^{4+}$ [27]. The Ti $2p_{1/2}$ band is placed 5.7 eV at higher binding energy, which corresponds with the spin-orbit-separation (sos). In the case of $TiO_2(90)$/LDPE composite, Ti $2p_{3/2}$ becomes broader, indicating the presence of a new contribution in the Ti 2p band. Peak deconvolution shows that the Ti 2p band can be reproduced using two doublets: one placed at 459.0 and 464.7 eV and a second one at 459.6 and 465.3 eV. The first doublet is placed at the same binding energy of the reference sample, indicating the presence of $Ti^{4+}$. The second doublet appears at the high binding energy side, clearly showing the existence of a new contribution $Ti^{x+}$, which can be related to the formation of Ti–O–C bonds in the $TiO_2$–LDPE interface. This component $Ti^{x+}$ has been observed previously in other titanium systems, as $TiO_2$–$SiO_2$ and $TiO_2$–$CeO_2$ [27–30]. The difference in the binding energies between $Ti^{4+}$ and $Ti^{x+}$ species has been attributed to a difference in the coordination number between the pure oxide (octahedrally coordinated) and the new compound (tetrahedrally coordinated). The increase in the binding energy can be due to an increase in the interatomic potentials produced by a decrease in the coordination number and a shortening of the
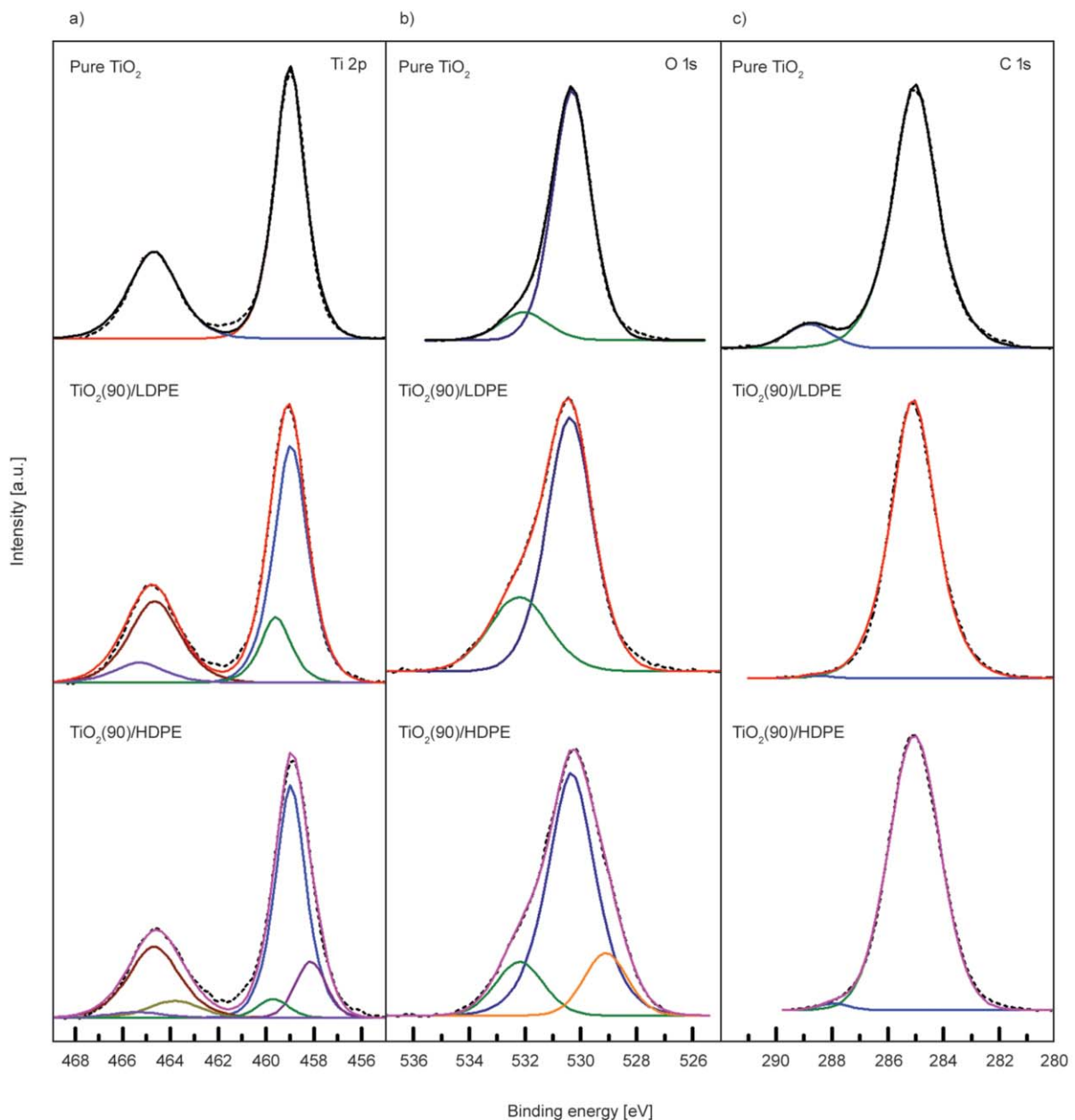


**Figure 5.** XPS high resolution spectra of pure $TiO_2$, $TiO_2(90)$/LDPE and $TiO_2(90)$/HDPE nanocomposites: Ti 2p band (a), O 1s band (b) and C 1s band (c)

Ti–O bonds. Tetrahedral titanium atoms make the titanium more electropositive and the Ti–O bond more ionic.

On the other hand, when the Ti 2p band of the $TiO_2(90)$/HDPE system was deconvoluted, three doublets were needed: one associated to $Ti^{4+}$, one related to $Ti^{x+}$, and a new component in the low binding energy size (458.2 and 463.9 eV). Li *et al.* [30] reported this last doublet in carbon-doped titania, suggesting that a $Ti^{3+}$ species was formed.

In the case of the O 1s band (Figure 5b), two different bands were distinguished: the one connected with Ti–O bonds (530.3 eV) and other band at 532.2 eV connected with O–C and OH–Ti bonds [31, 32]. In the case of $TiO_2(90)$/HDPE, a third band was observed at 529.1 eV related with O=C–OH bonds [33]. Both in the case of $TiO_2(90)$/LDPE and in $TiO_2(90)$/ HDPE samples, an increase in the band related with OH–Ti and O–C bonds was observed, as well as a shift from 532 to 532.2 eV. This shift could be related with changes in the chemical environment of the element or the presence of new chemical states with a binding energy near the one of OH–Ti and O–C bonds.

C 1s band (Figure 5c) presented a main peak at 285 eV in all the samples, with a widening in the case of $TiO_2(90)$/HDPE. This widening could be due to the presence of a small contribution of C–OH bonds, which appears at 286.4 eV [33].

Although both $TiO_2(90)$/LDPE and $TiO_2(90)$/HDPE catalysts presented the $Ti^{x+}$ component in the Ti 2p band, this contribution in the $TiO_2$/LDPE sample was higher (27% of the Ti 2p band) than in the $TiO_2$/HDPE sample (6% of the Ti 2p band). These results are consistent with the different photocatalytic response of these composites. The higher ionic character of $Ti^{x+}$ species in Ti–O–C bonds present in the $TiO_2$–polyethylene interface promotes electrons donation, then increasing the appearance of holes in the valence band. This would explain the increased activity of $TiO_2$–polyethylene nanocomposites in the degradation of MO under visible light comparing with pure $TiO_2$. Also based in the XPS analyses, the contribution of $Ti^{x+}$ was higher in $TiO_2(90)$/LDPE nanocomposite than in $TiO_2(90)$/HDPE, which could explain the higher effect of LDPE on the degradation activity.

In order to a better understanding of the photocatalytic activity of $TiO_2(90)$/LDPE nanocomposite and the interaction between $TiO_2$ and LDPE, room temperature photoluminescence (PL) measurements were carried out and studied in detail. The emission spectra of $TiO_2(90)$/LDPE, pure $TiO_2$ and LDPE are presented in Figure 6. For LDPE the corresponding
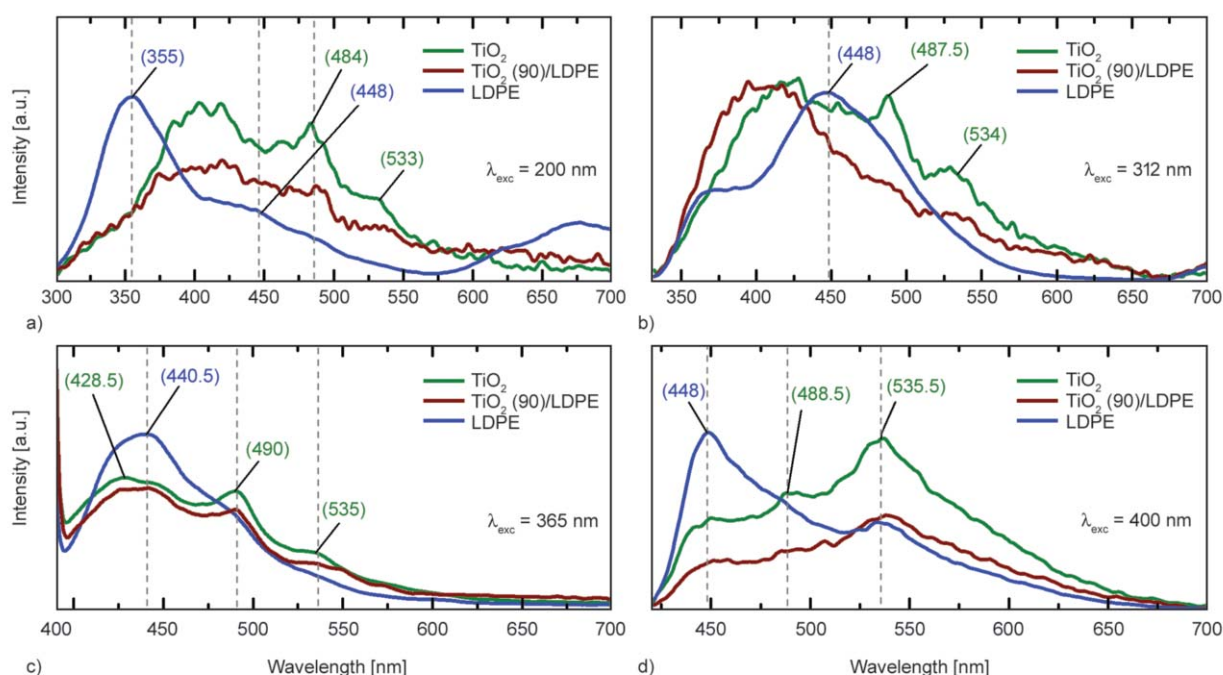


**Figure 6.** Room temperature photoluminescence spectra of the anatase $TiO_2$ nanoparticles, $TiO_2(90)$/LDPE, and LDPE excited at 200 nm (a), 312 nm (b), 365 nm (c), and 400 nm (d)

emission peaks were observed at 355 (3.5 eV) and ~448 nm (2.8 eV), while for TiO$_2$ and TiO$_2$(90)/LDPE the principal peaks were observed at 428 (2.9 eV), ~488 (2.5 eV), and 535 nm (2.3 eV). The samples were excited at 200 (6.2 eV), 312 (3.97 eV), 365 (3.4 eV) and 400 nm (3.1 eV). The only difference in the PL spectra of the samples was the intensity of the emission peaks. Nehate *et. al.* [34] reported that the emission in polyethylene polymer is due to groups attached in the monomer and the conversion of the hydroxyl (OH) group during the polymerization in the ester group. As well, they reported that the principal emission about 400 nm is associated with presence of chromophores, while peaks at ~360 and ~470 nm are due to O–H (bending) groups, C–H or –CH$_2$ (bending) chain. For TiO$_2$(90)/LDPE no change was observed in the shape and emission peaks of the PL spectra compared to the emission of the anatase TiO$_2$ nanoparticles. Thus, the variation in the intensities could be due to the difference in densities. A broad emission peak (pure TiO$_2$ nanoparticles) corresponding to the lowest indirect transition (428 nm (2.9 eV)) was also observed (Figure 6a, 6b). In addition, PL measurements revealed the presence of two shallow trap levels at energies of 2.5 (~488 nm) and 2.3 eV (535 nm), which were induced by the presence of the oxygen vacancies (Vo) [35]. The peak at 2.5 eV (~488 nm) in the sample is assigned to shallow trapped Vo associated with Ti$^{x+}$ centers below the conduction band [36, 37] and the peak at 2.3 eV (535 nm) is due to the transition between the mobile electrons and trapped holes [38]. However, the position of lower energy peaks/shoulders are the same in the TiO$_2$(90)/LDPE nanocomposite, indicating the same origin (oxygen vacancies, Vo) that in TiO$_2$ nanoparticles. Also we observed in Figure 6a, a broad emission in which the hydroxyl group (448 nm (2.8 eV)) could be immersed in the PL spectrum of the TiO$_2$(90)/LDPE sample. The presence of the hydroxyl group may form an acceptor level just above the valence band, favoring the photocatalytic activity. Also, the incorporation of TiO$_2$ nanoparticles in the LDPE could accelerate the photo-oxidation mechanism due to that TiO$_2$ can be excited at $\lambda_{exc} \leq 400$ nm to produce •OH radicals (see Figure 6) [39–42]. In addition, the increased relative surface area in TiO$_2$(90)/LDPE sample results in increased surface contact between the water molecules adsorbed on the material and the photocatalyst, allowing thus the production of chemisorbed surface
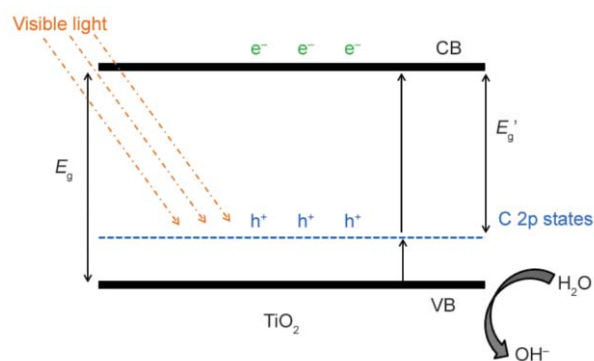


**Figure 7.** Schematic illustration showing the possible mechanism for photocatalytic degradation of organic pollutants

hydroxyl groups to produce •OH radicals. Moreover, the presence of OH species, as is shown in the PL spectra of TiO$_2$(90)/ LDPE sample, also contributes to the photo-production of •OH radicals. This result indicates a major concentration of C–OH groups supporting our findings about a photocatalytic behavior of samples.

The results presented in this work clearly suggest that the incorporation of C in the TiO$_2$ structure induces the formation of an acceptor impurity energy level above the valence band. Three C 2p bands lie within the band gap of TiO$_2$, thus reducing the energy gap from the valence to the conduction band ($E_g'$). This decrease in the energy gap extends the absorption spectrum to the visible light region (Figure 7). Additionally, the long term stability and reusability of the TiO$_2$(90)/LDPE sample was tested by recycling process. Figure 8 shows the recycling ability of this photocatalyst. After undergoing recycling process of methyl orange for three times under visible
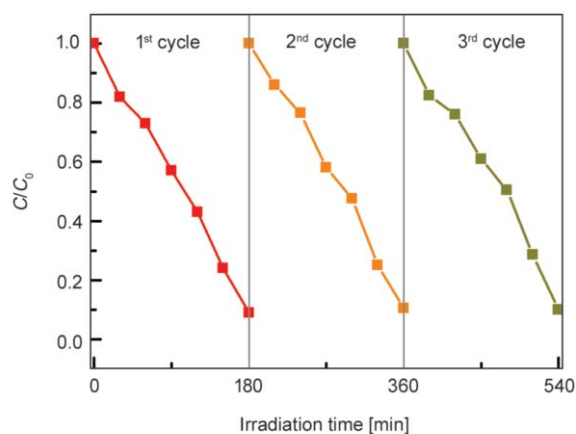


**Figure 8.** Degradation of methyl orange in the presence of the TiO$_2$(90)/LDPE catalyst under visible light for three cycles

light irradiation, very slight variation was found, being the efficiencies for the 1st, 2nd and 3rd cycle of 91, 89 and 90% respectively. Thus, it was concluded that the nanocomposite exhibits good stability and reusability for photocatalytic degradation of dyes under visible light irradiation.

As a final comment, it is worthwhile noting that these composites float on water. Thus, in addition to effectively improve the usage of light, especially in systems using solar irradiation, they could easily be recovered after the photocatalytic reaction, facilitating their applications to different types of contaminated water bodies [43, 44].

## 4. Conclusions

In summary, pure $TiO_2$ and $TiO_2$/LDPE and $TiO_2$/HDPE nanocomposites were successfully prepared by using a simple sol-gel method combined with polymer impregnation. All nanocomposites exhibited a lower bandgap than pure $TiO_2$, and were active in MO degradation under visible light. XRD analyses exhibited that synthesized $TiO_2$ presented characteristic anatase phase pattern, which not presented substantial changes during the preparation of the nanocomposites. XPS results suggested the formation of Ti–O–C bonds in the interface $TiO_2$–polyethylene, where higher ionic character of $Ti^{x+}$ species promotes electrons donation, increasing then the appearance of holes in the $TiO_2$ valence band. $TiO_2(90)$/LDPE nanocomposite presented the highest degradation efficiency of MO. These results were correlated to a higher contribution of $Ti^{x+}$ species in this sample compared to the other composites. Moreover, to explore the reaction mechanism of PE modified with $TiO_2$ for visible light response, the detection and behaviors of hydroxyl radical ($^•OH$) was discussed. Additionally, photoluminescence showed that $TiO_2(90)$/LDPE nanostructures contains relatively high concentrations of oxygen vacancies, which contributed to the photocatalytic properties of the nanomaterial. The results of the present work provide new insights about $TiO_2$–nanocomposites photocatalysts with notable visible light activity and stability that have interesting and potential environmental applications.

## References

[1] Khan M. M., Ansari S. A., Amal M. I., Lee J., Cho M. H.: Highly visible light active Ag@TiO2 nanocomposites synthesized using an electrochemically active biofilm: A novel biogenic approach. Nanoscale, **5**, 4427–4435 (2013).
https://doi.org/10.1039/c3nr00613a

[2] Khan M. M., Lee J., Cho M. H.: Au@TiO2 nanocomposites for the catalytic degradation of methyl orange and methylene blue: An electron relay effect. Journal of Industrial and Engineering Chemistry, **20**, 1584–1590 (2014).
https://doi.org/10.1016/j.jiec.2013.08.002

[3] Yuan J., Zhang X., Li H., Wang K., Gao S., Yin Z., Yu H., Zhu X., Xiong Z., Xie Y.: TiO2/SnO2 double-shelled hollow spheres-highly efficient photocatalyst for the degradation of rhodamine B. Catalysis Communications, **60**, 129–133 (2015).
https://doi.org/10.1016/j.catcom.2014.11.032

[4] Khan M. M., Ansari S. A., Pradhan D., Ansari M. O., Han D. H., Lee J., Cho M. H.: Band gap engineered TiO2 nanoparticles for visible light induced photoelectrochemical and photocatalytic studies. Journal of Materials Chemistry A, **2**, 637–644 (2014).
https://doi.org/10.1039/c3ta14052k

[5] Kalathil S., Khan M. M., Ansari S. A., Lee J., Cho M. H.: Band gap narrowing of titanium dioxide (TiO2) nanocrystals by electrochemically active biofilms and their visible light activity. Nanoscale, **5**, 6323–6326 (2013).
https://doi.org/10.1039/c3nr01280h

[6] Noimark S., Dunnill C. W., Parkin I. P.: Shining light on materials – A self-sterilising revolution. Advanced Drug Delivery Reviews, **65**, 570–580 (2013).
https://doi.org/10.1016/j.addr.2012.07.003

[7] Rekab K., Lepeytre C., Dunand M., Dappozze F., Herrmann J-M., Guillard C.: H2O2 and/or photocatalysis under UV-C irradiation for the removal of EDTA, a chelating agent present in nuclear waste waters. Applied Catalysis A: General, **488**, 103–110 (2014).
https://doi.org/10.1016/j.apcata.2014.09.036

[8] Suárez S., Arconada N., Castro Y., Coronado J. M., Portela R., Durán A., Sánchez B.: Photocatalytic degradation of TCE in dry and wet air conditions with $TiO_2$ porous thin films. Applied Catalysis B: Environmental, **108–109**, 14–21 (2011).
https://doi.org/10.1016/j.apcatb.2011.07.027

[9] Wang Y., Zhang J., Liu L., Zhu C., Liu X., Su Q.: Visible light photocatalysis of $V_2O_5/TiO_2$ nanoheterostructures prepared via electrospinning. Materials Letters, **75**, 95–98 (2012).
https://doi.org/10.1016/j.matlet.2012.01.074

[10] Mamane H., Horovitz I., Lozzi L., Di Camillo D., Avisar D.: The role of physical and operational parameters in photocatalysis by N-doped $TiO_2$ sol-gel thin films. Chemical Engineering Journal, **257**, 159–169 (2014).
https://doi.org/10.1016/j.cej.2014.07.018

[11] Venieri D., Gounaki I., Binas V., Zachopoulos A., Kiriakidis G., Mantzavinos D.: Inactivation of MS2 coliphage in sewage by solar photocatalysis using metal-doped $TiO_2$. Applied Catalysis B: Environmental, **178**, 54–64 (2015).
https://doi.org/10.1016/j.apcatb.2014.10.052

[12] Li J., Xu X., Liu X., Yu C., Yan D., Sun Z., Pan L.: Sn doped $TiO_2$ nanotube with oxygen vacancy for highly efficient visible light photocatalysis. Journal of Alloys and Compounds, **679**, 454–462 (2016).
https://doi.org/10.1016/j.jallcom.2016.04.080

[13] Ding Y., Zhang X., Chen L., Wang X., Zhang N., Liu Y., Fang Y.: Oxygen vacancies enabled enhancement of catalytic property of Al reduced anatase $TiO_2$ in the decomposition of high concentration ozone. Journal of Solid State Chemistry, **250**, 121–127 (2017).
https://doi.org/10.1016/j.jssc.2017.03.022

[14] Cámara R. M., Crespo E., Portela R., Suárez S., Bautista L., Gutiérrez-Martín F., Sánchez B.: Enhanced photocatalytic activity of $TiO_2$ thin films on plasma-pretreated organic polymers. Catalysis Today, **230**, 145–151 (2014).
https://doi.org/10.1016/j.cattod.2013.10.049

[15] Li X., He G., Han Y., Xue Q., Wu X., Yang S.: Magnetic titania-silica composite-polypyrrole core-shell spheres and their high sensitivity toward hydrogen peroxide as electrochemical sensor. Journal of Colloid and Interface Science, **387**, 39–46 (2012).
https://doi.org/10.1016/j.jcis.2012.07.071

[16] Li X., Jiang G., He G., Zheng W., Tan Y., Xiao W.: Preparation of porous $PPyTiO_2$ composites: Improved visible light photoactivity and the mechanism. Chemical Engineering Journal, **236**, 480–489 (2014).
https://doi.org/10.1016/j.cej.2013.10.057

[17] Huo P., Yan Y., Li S., Li H., Huang W.: Floating photocatalysts of fly-ash cenospheres supported $AgCl/TiO_2$ films with enhanced Rhodamine B photodecomposition activity. Desalination, **256**, 196–200 (2010).
https://doi.org/10.1016/j.desal.2010.01.012

[18] Długosz M., Żmudzki P., Kwiecień A., Szczubiałka K., Krzek J., Nowakowska M.: Photocatalytic degradation of sulfamethoxazole in aqueous solution using a floating $TiO_2$-expanded perlite photocatalyst. Journal of Hazardous Materials, **298**, 146–153 (2015).
https://doi.org/10.1016/j.jhazmat.2015.05.016

[19] Saravanan R., Shankar H., Prakash T., Narayanan V., Stephen A.: ZnO/CdO composite nanorods for photocatalytic degradation of methylene blue under visible light. Materials Chemistry and Physics, **125**, 277–280 (2011).
https://doi.org/10.1016/j.matchemphys.2010.09.030

[20] Wang C-L., Hwang W-S., Chu H-L., Lin H-J., Ko H-H., Wang M-C.: Kinetics of anatase transition to rutile $TiO_2$ from titanium dioxide precursor powders synthesized by a sol-gel process. Ceramics International, **42**, 13136–13143 (2016).
https://doi.org/10.1016/j.ceramint.2016.05.101

[21] Carotenuto G., De Nicola S., Palomba M., Pullini D., Horsewell A., Hansen T. W., Nicolais L.: Mechanical properties of low-density polyethylene filled by graphite nanoplatelets. Nanotechnology, **23**, 485705/1–485705/8 (2012).
https://doi.org/10.1088/0957-4484/23/48/485705

[22] Madani M.: Structure, optical and thermal decomposition characters of LDPE graft copolymers synthesized by gamma irradiation. Bulletin of Materials Science, **33**, 65–73 (2010).
https://doi.org/10.1007/s12034-010-0009-9

[23] Grigoriadou I., Paraskevopoulos K. M., Chrissafis K., Pavlidou E., Stamkopoulos T-G., Bikiaris D.: Effect of different nanoparticles on HDPE UV stability. Polymer Degradation and Stability, **96**, 151–163 (2011).
https://doi.org/10.1016/j.polymdegradstab.2010.10.001

[24] Liu H., Liu J., Zhou Q., Wang J.: Novel polymer electrolyte based on PVDF/HDPE blending for lithium-ion battery. Materials Letters, **99**, 164–167 (2013).
https://doi.org/10.1016/j.matlet.2013.03.033

[25] Mosquera E., del Pozo I., Morel M.: Structure and red shift of optical band gap in CdO–ZnO nanocomposite synthesized by the sol gel method. Journal of Solid State Chemistry, **206**, 265–271 (2013).
https://doi.org/10.1016/j.jssc.2013.08.025

[26] Mosquera E., Carvajal N.: Low temperature synthesis and blue photoluminescence of ZnS submicronparticles. Materials Letters, **129**, 8–11 (2014).
https://doi.org/10.1016/j.matlet.2014.05.037

[27] Benito N., Palacio C.: Growth of Ti–O–Si mixed oxides by reactive ion-beam mixing of Ti/Si interfaces. Journal of Physics D: Applied Physics, **47**, 015308/1–015308/7 (2014).
https://doi.org/10.1088/0022-3727/47/1/015308

[28] Luan Z., Maes E. M., van der Heide P. A. W., Zhao D., Czernuszewicz R. S., Kevan L.: Incorporation of titanium into mesoporous silica molecular sieve SBA-15. Chemistry of Materials, **11**, 3680–3686 (1999).
https://doi.org/10.1021/cm9905141

[29] Suzana M., Francisco P., Mastelaro V. R., Nascente P. A. P., Florentino A. O.: Activity and characterization by XPS, HR-TEM, Raman spectroscopy, and BET surface area of CuO/CeO$_2$–TiO$_2$ catalysts. The Journal of Physical Chemistry B, **105**, 10515–10522 (2001). https://doi.org/10.1021/jp0109675

[30] Li Y., Hwang D-S., Lee N. H., Kim S-J.: Synthesis and characterization of carbon-doped titania as an artificial solar light sensitive photocatalyst. Chemical Physics Letters, **404**, 25–29 (2005). https://doi.org/10.1016/j.cplett.2005.01.062

[31] El Mel A. A., Angleraud B., Gautron E., Granier A., Tessier P. Y.: XPS study of the surface composition modification of nc-TiC/C nanocomposite films under *in situ* argon ion bombardment. Thin Solid Films, **519**, 3982–3985 (2011). https://doi.org/10.1016/j.tsf.2011.01.200

[32] Zhao X., Li Z., Chen Y., Shi L., Zhu Y.: Solid-phase photocatalytic degradation of polyethylene plastic under UV and solar light irradiation. Journal of Molecular Catalysis A: Chemical, **268**, 101–106 (2007). https://doi.org/10.1016/j.molcata.2006.12.012

[33] Yang D., Velamakanni A., Bozoklu G., Park S., Stoller M., Piner R. D., Stankovich S., Jung I., Field D. A., Ventrice Jr. C. A., Ruoff R. S.: Chemical analysis of graphene oxide films after heat and chemical treatments by X-ray photoelectron and Micro-Raman spectroscopy. Carbon, **47**, 145–152 (2009). https://doi.org/10.1016/j.carbon.2008.09.045

[34] Nehate A. K., Joshi T. R., Rajput S., Savita H.: Luminescence and thermoluminescence study of polyethylene polymer (LLDPE, LDPE, HDPE). Journal of Photochemistry and Photobiology A: Chemistry, **74**, 279–282 (1993). https://doi.org/10.1016/1010-6030(93)80127-U

[35] Morgan B. J., Watson G. W.: Intrinsic n-type defect formation in TiO$_2$: A comparison of rutile and anatase from GGA+U calculations. The Journal of Physical Chemistry C, **114**, 2321–2328 (2010). https://doi.org/10.1021/jp9088047

[36] Tshabalala Z. P., Motaung D. E., Mhlongo G. H., Ntwaeaborwa O. M.: Facile synthesis of improved room temperature gas sensing properties of TiO$_2$ nanostructures: Effect of acid treatment. Sensors and Actuators B: Chemical, **224**, 841–856 (2016). https://doi.org/10.1016/j.snb.2015.10.079

[37] Santara B., Giri P. K., Imakita K., Fujii M.: Evidence for Ti interstitial induced extended visible absorption and near infrared photoluminescence from undoped TiO$_2$ nanoribbons: An *in situ* photoluminescence study. The Journal of Physical Chemistry C, **117**, 23402–23411 (2013). https://doi.org/10.1021/jp408249q

[38] Tachikawa T., Majima T.: Single-molecule, single-particle fluorescence imaging of TiO$_2$-based photocatalytic reactions. Chemical Society Reviews, **39**, 4802–4819 (2010). https://doi.org/10.1039/B919698F

[39] Saravanan R., Sacari E., Gracia F., Khan M. M., Mosquera E., Gupta V. K.: Conducting PANI stimulated ZnO system for visible light photocatalytic degradation of coloured dyes. Journal of Molecular Liquids, **221**, 1029–1033 (2016). https://doi.org/10.1016/j.molliq.2016.06.074

[40] Saravanan R., Karthikeyan N., Gupta V. K., Thirumal E., Thangadurai P., Narayanan V., Stephen A.: ZnO/Ag nanocomposite: An efficient catalyst for degradation studies of textile effluents under visible light. Materials Science and Engineering: C, **33**, 2235–2244 (2013). https://doi.org/10.1016/j.msec.2013.01.046

[41] Rajendran S., Khan M. M., Gracia F., Qin J., Gupta V. K., Arumainathan S.: Ce$^{3+}$-ion-induced visible-light photocatalytic degradation and electrochemical activity of ZnO/CeO$_2$ nanocomposite. Scientific Reports, **6**, 31641/1–31641/11 (2016). https://doi.org/10.1038/srep31641

[42] Saravanan R., Gupta V. K., Mosquera E., Gracia F.: Preparation and characterization of V$_2$O$_5$/ZnO nanocomposite system for photocatalytic application. Journal of Molecular Liquids, **198**, 409–412 (2014). https://doi.org/10.1016/j.molliq.2014.07.030

[43] Magalhães F., Lago R. M.: Floating photocatalysts based on TiO$_2$ grafted on expanded polystyrene beads for the solar degradation of dyes. Solar Energy, **83**, 1521–1526 (2009). https://doi.org/10.1016/j.solener.2009.04.005

[44] Wang X., Wang W., Wang X., Zhang J., Gu Z., Zhou L., Zhao J.: Enhanced visible light photocatalytic activity of a floating photocatalyst based on B–N-codoped TiO$_2$ grafted on expanded perlite. RSC Advances, **5**, 41385–41392 (2015). https://doi.org/10.1039/C5RA06056G